Journal of The Electrochemical Society, **158** (9) K175-K182 (2011)
0013-4651/2011/158(9)/K175/8/$28.00 © The Electrochemical Society

Transport Characterization of Chemically-Functionalized Single-Walled Carbon Nanotube Thin Film Transistor

Jung-Ah Lee,[a,b] Kyeong-Kap Paek,[c] Sangyoup Lee,[a] Byeong-Kwon Ju,[d] Yun-Hi Lee,[b] and Hyun Joon Shin[a,z]

[a]*Nano-Bio Photonics Lab., Biomedical Science Center, Korea Institute of Science and Technology, Seongbuk-gu, Seoul 136-791, Korea*
[b]*Department of Physics, Korea University, 5-1, Anam-dong, Seongbuk-gu, Seoul 136-713, Korea*
[c]*Department of Electronic Engineering, Daejin University, Pocheon, Gyeonggi-do 487-711, Korea*
[d]*School of Electrical Engineering, Korea University, 5-1, Anam-dong, Seongbuk-gu, Seoul 136-713, Korea*

The electronic transport properties of the thin film transistor (TFT) devices consisting of carboxyl-modified single-walled carbon nanotube (c-SWCNT) network are studied. This work is focused on the analysis of the effect of chemical treatment on the electronic transport properties from these devices. The c-SWCNT thin film transistor (c-SWCNT TFT) devices were fabricated by a directed assembly method based on electrostatic interaction between amino-functionalized substrate and c-SWCNTs. The electrical characteristics of c-SWCNT TFTs were measured at room temperature. From the Raman results and the transport characteristics of c-SWCNT TFT devices, the transport mechanism in these devices can be accounted that the deep levels arising from vacancy-adatom complex induced the changes in the electronic band structure of SWCNTs.
 [DOI: 10.1149/1.3610343]

Manuscript submitted December 31, 2010; revised manuscript received June 6, 2011. Published July 15, 2011.

Single-walled carbon nanotube (SWCNT) thin film has been suggested as an excellent candidate for various applications because of its flexibility, electrical conductivity, and optical transparency. The recent studies of SWCNT thin film are described about the possibility of realization of transparent conductive coatings, transparent thin film transistors (TFTs), photovoltaic cells, biochemical sensors, flexible display, and transparent flexible sensors.[1–13]

SWCNT thin film is fabricated by using either thermal chemical vapor deposition or solution-based deposition methods. The solution-based deposition methods include spray coating, dip coating, transfer printing, layer-by-layer, and Langmuir-Blodgett deposition method. As a precondition for these methods, SWCNT must be prepared as a suspension. The most commonly employed process for the preparation of SWCNT suspension is a chemical oxidation reaction using strong acids or oxidizing agents. The SWCNT suspension prepared by chemical treatment can be used as a raw material for the production of SWCNT thin film. The SWCNT thin film obtained by methods mentioned above can be used in a wide variety of applications ranging from nanoelectronics to biological systems.

As one of the most fundamental features, the conductivity of SWCNT thin film has been investigated by using field effect transistors (FETs) from numerous groups.[8,14] The major conclusion obtained from their results is that the conductivity of SWCNT network is dependent on the combination of conditions such as length, diameter, and chirality of the respective SWCNTs as well as their interactions within the network, such as tube contact angle, packing density, and orientation.[14]

The electrical transport characteristics of SWCNT thin film with different functional groups have been also analyzed using FET structures.[15] Noor's group measured conductance changes by using interaction between carboxylated SWCNT (c-SWCNT) and biological molecules.[16] Mäklin et al. have demonstrated the possibility for gas sensor through the electrical transport measurement from the c-SWCNT thin film transistor (c-SWCNT TFT) obtained by inkjet-printing technique.[17] Besides, Mustonen et al. as a member of the same group analyzed the transport mechanism from the c-SWCNT films with various densities.[18]

Zhang's group performed the study of transport mechanism from acid-treated SWCNT TFTs by combining Raman spectroscopy with transistor transfer characteristics.[19] Their results demonstrated that the disappearance of gating effect is caused by bandgap changes induced by oxidative absorbates on the semiconducting SWCNTs (s-SWCNTs).

[z] E-mail: kaiphy@kist.re.kr

However, in spite of numerous efforts to elucidate the transport mechanism, the electrical properties on the c-SWCNT films remain unresolved by the lack of relevant research.

In this work, the c-SWCNT TFT devices were fabricated by the combination of conventional lithographic technique with the self-assembled monolayer technique. The transport mechanism of c-SWCNT TFT devices is investigated, based on both the electrical properties from these devices and the structural properties from pristine and c-SWCNT samples by Raman spectroscopy.

Experimental

The c-SWCNT TFT devices were fabricated in two steps. The first step is to prepare a c-SWCNT suspension. In the second step, the modification on the surface of a substrate and the fabrication of TFT devices are carried out.

First, the procedure for making the c-SWCNT suspension consists of an oxidation in strong acids and filtration. The raw material used in making the suspension was a pristine SWCNT (p-SWCNT) commercially produced by both the arc-discharge and purification methods (Iljin Nanotec. CO. Ltd., Korea). The p-SWCNTs (10 mg) were suspended in a mixture of 40 ml of nitric and sulfuric acids with a volume ratio of 1:3. The mixture was stirred for 48 h at room temperature and sonicated for 10 h using a water bath sonicator (40 kHz, 185 W, Branson ultrasonic cleaner 5510). After the oxidation reaction, the oxidation product was diluted with 200 ml of distilled water. The diluted solution was filtered through a 0.2 μm pore size membrane filter (Millipore, Ireland) by suction with a vacuum aspirator. Then, a thick SWCNT mat was formed as a precipitate on the membrane filter. The SWCNT mat was repeatedly washed using 10 mM sodium hydroxide solution and distilled water until the *p*H of the mat was 7. After being washed, the SWCNT mat was separated from the filter in distilled water by sonication, and the resulting mixture was stirred at room temperature for 1 h to get a homogeneous solution. Subsequently, the well-dispersed status of SWCNT suspension was prepared. Until now, this procedure is to introduce the carboxyl group (-COOH) onto the surface of nanotubes, as well as to convert the hydrophobic surface of CNTs into the hydrophilic one.[20] The presence of carboxylic group on the surface of the acid-treated SWCNT was confirmed by Fourier transform infrared spectroscopy as described in our previous paper.[21] The prepared c-SWCNT suspension was again diluted with distilled water for the control of concentration. The optimized ranges of c-SWCNT suspension concentration obtained from our experiments were from 0.03 to 0.192 mg/ml. This result is similar with the results of the

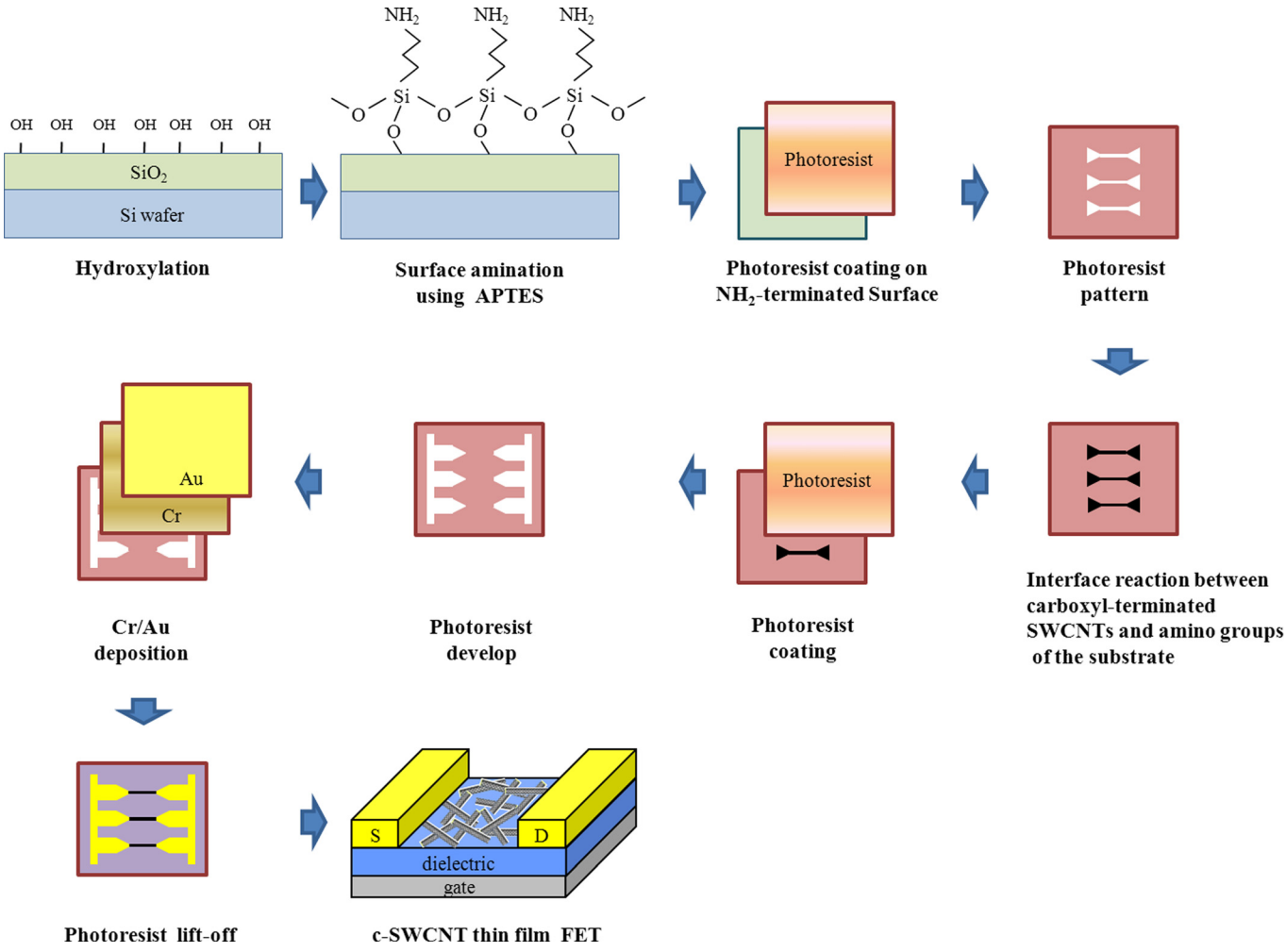

Figure 1. (Color online) Schematic showing each step in the fabrication process for c-SWCNT thin film transistor.

Zhao's paper.[22] The final concentrations of c-SWCNT suspension for c-SWCNT TFT device fabrication were controlled into three types such as 0.10, 0.15, and 0.192 mg/ml.

Second, the fabrication of c-SWCNT TFT devices started with the surface modification of a substrate. The substrate used in the experiment was a heavily doped p-type Si (100) wafer with a silicon dioxide layer of 500 nm grown by wet oxidation. Prior to the photolithography process to define device patterns, the introduction of hydroxyl group onto the SiO_2/Si substrate in Fig. 1 was achieved by the following procedure: (1) immersed in the APM solution (NH_4OH:H_2O_2:H_2O = 1:1:7) at 85 °C for 8 min; (2) rinsed with an amount of distilled water; (3) after dried using N_2 gas.

After the hydroxylation reaction, the surface modification on the hydroxylated substrate as the second step of Fig. 1 was performed by using 3-aminopropyltriethoxysilane (APTES, Sigma-Aldrich). For the formation of amino group, the hydroxylated substrate was immersed into a solution of 2% APTES in 95% ethanol/water at ~60 °C for 10 min. Then, the substrate was rinsed thoroughly with absolute ethanol and dried in vacuum. Through this reaction process using APTES as a self-assembled monolayer (SAM), the amino group was introduced onto the substrate surface. The substrate modified with APTES SAM was characterized with a contact angle analyzer (SEO Phoenix 450, Surface Electro Optics Corporation Ltd., Korea) using a sessile drop method. Besides, the contact angle on Au electrode was measured for the contact resistance. All measurements using distilled water as test liquid were repeated 5 times for the reproducibility of contact angle values.

The c-SWCNT TFT devices depicted in Fig. 1 were fabricated with a device structure using a back gate electrode. As already mentioned above, the substrate with a 500- nm -thick SiO_2 layer used in the surface treatment was employed as a back gate. The channel length and width of the FET devices were 2 and 2 μm, respectively. After the first patterning by a photolithography process, the c-SWCNT thin films were deposited on the APTES-modified position of the photoresist-patterned substrate. The thin films were fabricated by a drop casting method with a same volume of 20 μl extracted from the three kinds of c-SWCNT suspensions. As the solution dried, the second patterning to determine the position of the electrode was achieved. A layer of Au/Cr (100 nm/10 nm) on the source and drain electrodes was deposited by an electron-beam evaporation method. Then, a lift-off process was performed to open a new window for the adsorbed c-SWCNT layer in channel area. Especially, this process done in acetone was aided by ultrasonic excitation for removal of photoresist and the electrode materials. After thoroughly rinsed with sufficient volume of water, the c-SWCNT TFT device was finally completed.

To monitor the structural changes of the acid-treated CNTs, the p-SWCNT and c-SWCNT samples were characterized by the Raman spectroscopy (Horiba Jobin Yvon HR 800 UV Raman spectrometer). Field emission scanning electron microscopy (FE-SEM) was employed to image the distribution of c-SWCNT thin films on a SiO_2/Si substrate (FEI Nova NanoSEM200). The electrical characterization of the fabricated c-SWCNT TFTs was performed on ~90 devices by using semiconductor characterization system (Keithley 4200-SCS) in ambient air and at room temperature. Each sample

was measured on a probe station equipped with a conductive vacuum chuck for a back-gate contact. The gate voltage was applied to the back of the Si substrate.

Results and Discussion

Figure 1 shows a schematic illustration of the fabrication process for the c-SWCNT TFT devices. In this figure, the hydroxyl groups on the substrate surface were used as anchor for the formation of the APTES SAM acting as an intermediate molecule. The surface modification by APTES was carried out for the chemical bonding between carboxyls of SWCNTs and hydroxyls of the SiO_2 surface. After the formation of APTES layers, the c-SWCNTs were assembled onto the substrate by the electrostatic interaction between the amine and carboxylic groups.[23]

To estimate the change in the interface due to the surface modification, the measurement of the contact angles was performed. The water contact angles on the APTES-treated surface and SiO_2 substrate were observed as 60.5 and 21°, respectively. From the fact that the contact angles of the amino-terminated surface reported from the literature are approximately varied in the range of 60–70°, it can be inferred that the measured water contact angles on the APTES layer were similar to the literature data.[24–26] Therefore, this method was adopted for the surface modification of the substrate.

Figure 2 shows the Raman spectra for p-SWCNT and c-SWCNT before and after the acid treatment. The Raman result in Fig. 2a shows the full range Raman spectra taken from the two samples, and that in Fig. 2b represents the enlarged image of the radial breathing mode (RBM) region in Fig. 2a. As shown in Fig. 2b, the RBM peak of c-SWCNT (182 cm^{-1}) was observed at high frequency than that of p-SWCNT (177 cm^{-1}). This result is consistent with that obtained from the experiments using other oxidation methods.[20,27–31] The origin for the shift of the RBM frequency presented in this figure is considered to be produced by the dopant insertion into the nanotubes.[31,32] However, in the experimental procedure of this paper, no dopants were added to the nanotube.

For a more specific approach, the G band in Fig. 2c was also examined. The G band in this figure was observed with two split components of the G^- and G^+ peaks for each sample. The G^- peak located at ~1569 cm^{-1} did not show the clear difference between p-SWCNT and c-SWCNT. The G^+ peak of c-SWCNT at 1596 cm^{-1} was found to be located at high frequency than that of p-SWCNT at 1581 cm^{-1}. This result on the c-SWCNT (1596 cm^{-1}) is identified as the signal for the semiconducting component, which is similar to the previous reports.[20,33–35] Besides, the fact that the G^+ peak intensity is higher than that of G^- peak corresponds to the characteristics of s-SWCNTs.[20,33–35]

Based on the previous studies, the important point that can be drawn from this result is that the G band shift is associated with the charge transfer between nanotubes and intercalated molecules or absorbed atoms acting as the dopants.[34–36] The types of charge transfer between dopants and SWCNT are determined by the direction of the G^+ peak shift.[37–39] Concretely, the charge transfer resulting from dopant additions to SWCNTs is given as follows: n-type doping induced a downshift of the G^+ band, on the other hand, p-type doping induced an upshift of the G^+ band.[34,35] Therefore, it is possible to infer that our c-SWCNT sample is governed by the p-type doping behavior due to the upshift of G band.

Based on the analysis on the Raman results in Fig. 2, we tried to explain both the RBM shift occurred without additional dopants and the charge-transfer process from the G band shift. If these subjects are considered with the theoretical aspects, the RBM frequency is applicable to the structural identification of nanotubes, and the charge-transfer process is relevant to the electrical properties of FET devices.[40–42]

According to the background mentioned above, Raman spectroscopy and TFT device were used to observe the structural and electrical properties of c-SWCNT. The TFT devices with c-SWCNT thin film were fabricated by using the three kinds of c-SWCNT suspensions (0.10, 0.15, 0.192 mg/ml), and the fabricated devices were denoted as FET-1, FET-2, and FET-3, respectively.

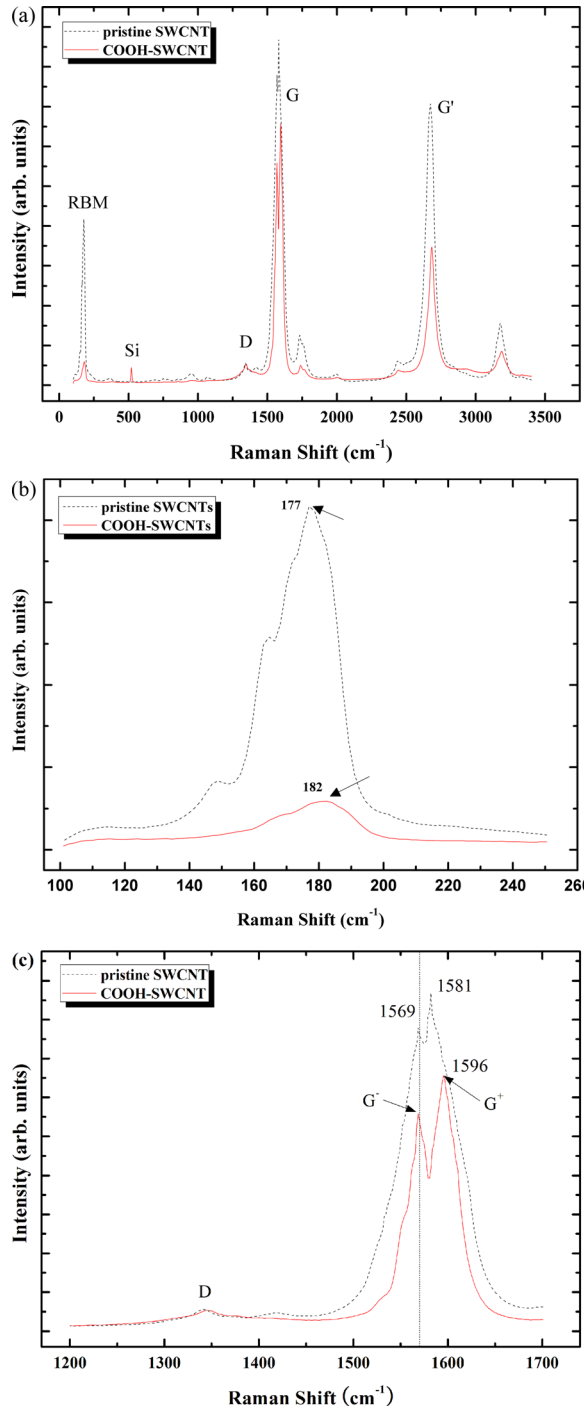

Figure 2. (Color online) The Raman spectra from pristine SWCNT and c-SWCNT using a laser of wavelength of $\lambda = 514$ nm. (a) full range Raman spectra (100–3500 cm^{-1}), (b) RBM region (100–260 cm^{-1}), and (c) D and G band region (1200–1700 cm^{-1}).

Figure 3 presents the FE-SEM images of c-SWCNT thin films made using suspensions of three different concentrations. Each tube in Fig. 3a and 3b (0.10 and 0.15 mg/ml) were observed with the appearance of isolated or grouped bundles with the intersection points. The presence of c-SWCNT bundles can be attributed to attractive interaction due to van der waals forces between adjacent nanotubes during the reaction process. The uncovered regions on the substrate were visible in both images. The SEM image in Fig. 3c

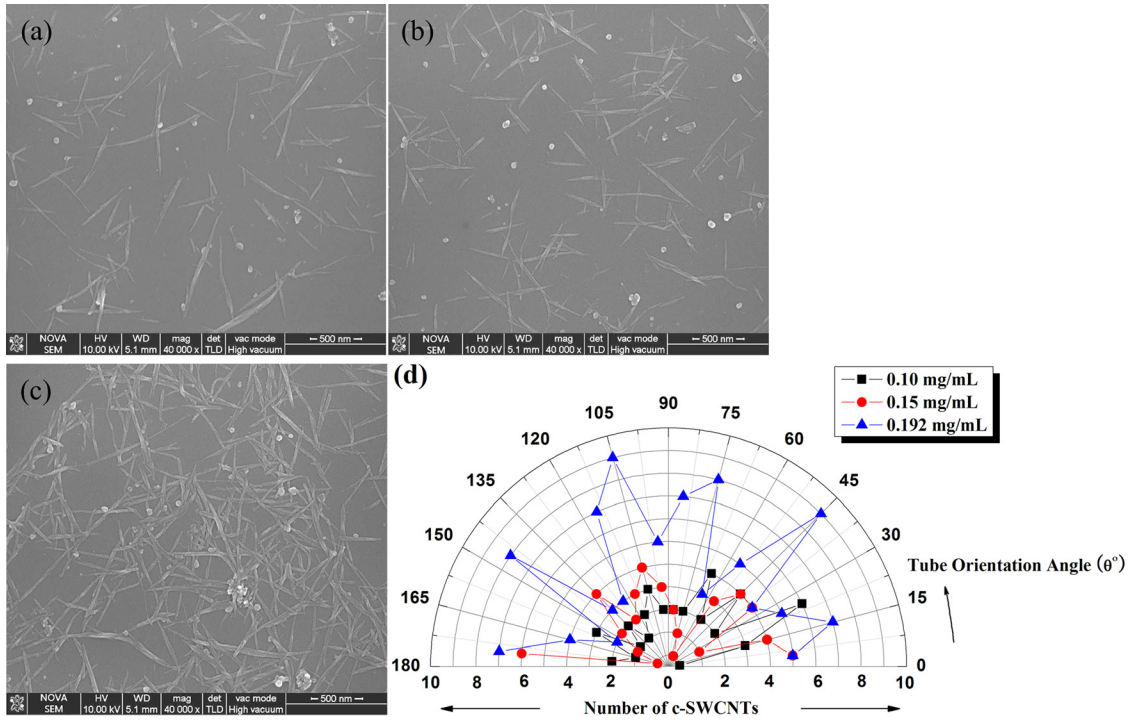

Figure 3. (Color online) SEM images on the c-SWCNT films deposited on a SiO_2/Si surface using the procedure described in Fig. 1: (a) 0.10 mg/ml, (b) 0.15 mg/ml, (c) 0.192 mg/ml, and (d) tube orientation. The plots in part (d) show distribution functions for the tube orientation angles (θ°) determined from the analysis of the SEM images.

(0.192 mg/ml) shows the formation of a more densely packed layer than the cases in Figs. 3a and 3b.

From the observation of all SEM images, it can be noticed that the surface coverage of randomly positioned c-SWCNTs is proportional to the concentration of c-SWCNT suspension. Besides, the surface state of the films displayed that some impurities were located in their surface. The impurities were shown to be produced in the reaction process with the acids for the functionalization of SWCNT. As the byproduct of the oxidation using strong acids, the impurities can be classified into the two types as follows. One is a material such as carboxylated carbonaceous fragments (CCFs) as an aggregate of the carbon pieces apart from the SWCNT by the acid attack.[43] The other is molecules called vacancy-carboxyl pairs (VCPs), which are produced by a strong covalent bond between vacancies located in the skeleton of SWCNT and the COOH groups induced during the oxidation process.[44]

The impurity molecules described above, as the intercalated molecules into the defects of the nanotubes, has been speculated to degrade the electrical performance of the devices through increasing the electrode-nanotube resistance or the local electrostatic environments of SWCNTs.[45,46]

As different types of impurities, the contaminants adsorbed on the surface of SWCNT in the device fabrication process can also vary the contact resistance by acting as tunnel barriers at the electrodes or causing poor wetting of the electrode metallization. Because of these concerns, the measurements on the electrical properties of the devices were performed after thoroughly rinsed with water to minimize the effects of the contaminants.

Next, Fig. 3d represents the orientation of the c-SWCNTs obtained from the SEM images from 3a to 3c. The orientation of the nanotubes appeared to be spread over a broad range of angle's value, according to the increase of the nanotubes concentration.

As can be seen in these images associated with the nanotube alignment, the junctions between the nanotubes appeared to be proportional to the increase of the surface coverage due to the increase of the c-SWCNTs concentration. Therefore, this result suggests that the contact resistances resulting from these junctions act as one of the constraints on the conduction paths located between electrodes.

Figure 4 shows the electrical properties of the FET-1 and FET-2 devices. In the Fig. 4, Figs. 4a and 4c indicate the characteristics of drain current versus drain voltage ($I_{DS}-V_{DS}$) by tuning the gate voltages obtained from each device. The $I_{DS}-V_G$ characteristics for the two devices are displayed in Figs. 4b and 4d.

The two devices in the $I_{DS}-V_{DS}$ curves of the Figs. 4a and 4c, despite of the difference of concentration of the c-SWCNT, were observed to follow a weak-metallic behavior. This transport behavior can be accepted as a suitable result when the metallic components of SWCNTs (m-SWCNTs) were connected with electrodes. To confirm the composition of c-SWCNT thin film located between electrodes, the Raman results in Fig. 2 were reconsidered. The RBM peak (182 cm^{-1}) in Fig. 2b and the G peak result in Fig. 2c are estimated to correspond to the characteristics of s-SWCNTs.[20,27,28,33,34] From these results, it can be deduced that the c-SWCNT sample consists of nearly the s-SWCNTs after the acid treatment. This opinion can be verified by the optical absorption spectra shown in Ref. 21. Therefore, the transport behavior in Fig. 4a and 4c can be explained as produced by the s-SWCNTs with COOH groups.

Figure 4b shows the $I_{DS}-V_G$ curves obtained from the FET-1 and FET-2 devices when V_{DS} is 200 mV. Figure 4d shows the $I_{DS}-V_G$ characteristics from the FET-2 devices measured at various drain voltages.

In Fig. 4b, the upper curve for the FET-1 devices represents the ambipolar transport properties. This transport behavior is a distinguishing feature from the results in lower curve given as a form of incompletely depleted curves within the gate sweeping range, as shown in Fig. 4d. The ambipolar transport characteristics of the upper curve indicate that the schottky barriers at source and drain have similar transparencies for hole and electron tunneling. The charge carrier source for the transport properties can be understood by considering the charge transfer in both c-SWCNT and APTES. The first reason of the behavior is that the n-type behavior comes from the electron donation by the amine group on APTES.[41] The

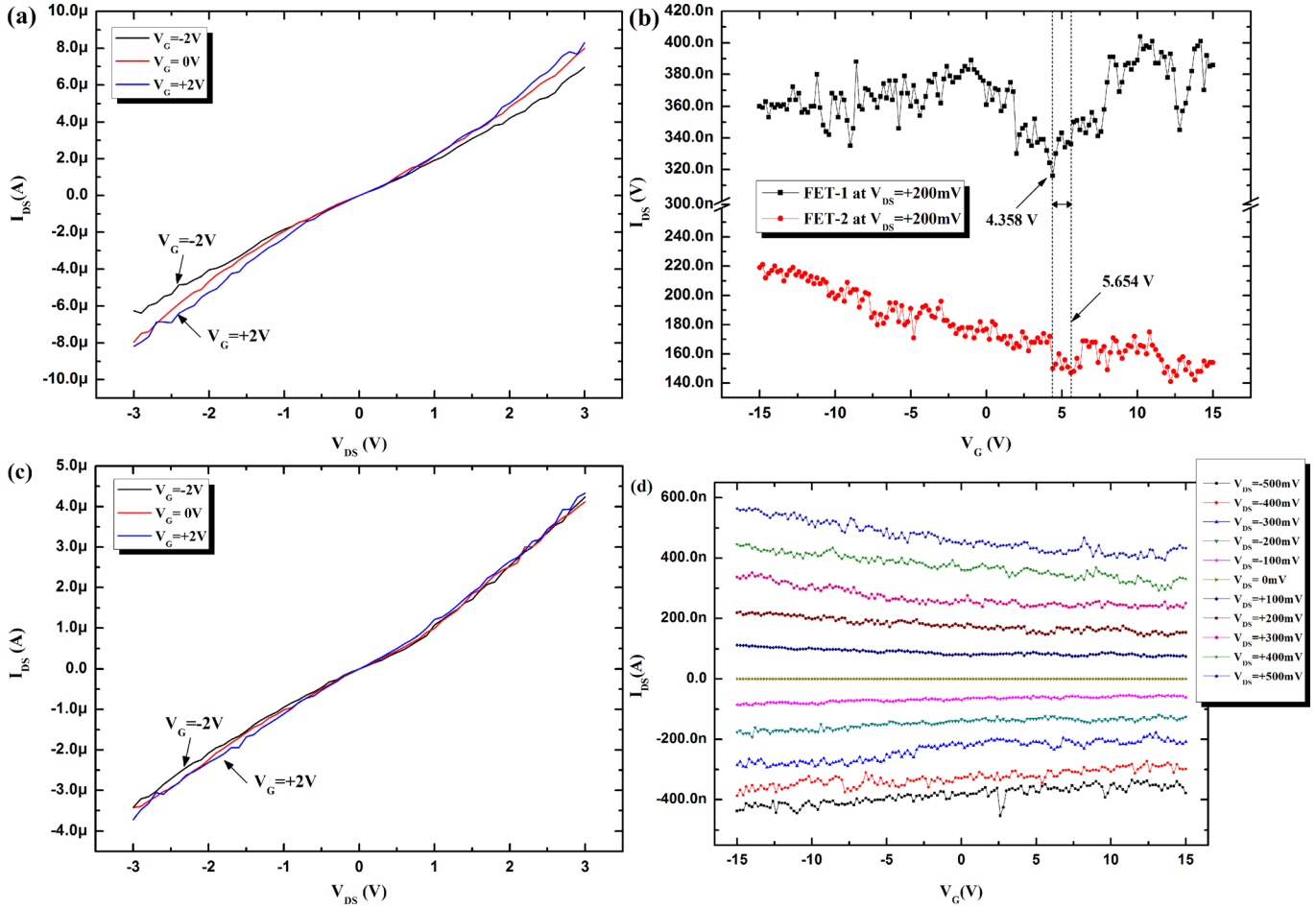

Figure 4. (Color online) The electrical characteristics for c-SWCNT thin film transistors produced using suspensions with concentrations of 0.10 and 0.15 mg/ml. (a) current-voltage characteristics between source and drain electrodes, (b) current-gate voltage characteristics (FET-1 device), (c) current-voltage characteristics between source and drain electrodes, (d) current-gate voltage characteristics (FET-2 device).

second reason is that the c-SWCNT exhibits the p-type behavior by hole-carriers.[42] Thus, the result of the FET-1 devices in Fig. 4b were explained as the transport characteristics arising from both electron-carriers by amine group and hole-carriers by c-SWCNT.

Meanwhile, the lower curve for the FET-2 device shows the p-type behavior in contrast to the transport properties of the FET-1 device. Especially, the threshold voltage V_{th} of p-channel in this curve appears to shift from 4.358 to 5.654 V. This shift indicates that the main carriers are converted as p-type carriers with increase of the c-SWCNT concentration. This also implies that the holes in the nanotubes with carboxylic groups play a more important role in the transport behavior than the electrons donated from the amine-containing molecules.

When the upper and lower curves are compared for more detailed study, the I_{DS} for the lower curve shows a tendency to decrease than that for the upper curve. This result can be explained by the factors relevant to the formation of the current paths between the electrodes and nanotubes. As described in Fig. 3, the current paths can be changed by various molecules (vacancy-related defects, CCFs, other contaminants, etc) located on both the nanotube surface and the c-SWCNT TFTs.[43,47] The molecules found in both the device and the nanotube surface can act as a factor to modify the gate potential and can also alter the conductivity of the c-SWCNT TFT.

The logical reason introduced to explain the decrease of I_{DS} is that the conductivity of the c-SWCNT TFT is associated with its carrier mobility and carrier density.[48]

First, based on the fact that the I_{DS} was decreased by the increase of the concentration of both c-SWCNT and impurity molecules, one can assume that the result is attributed to the interaction between the molecules and randomly distributed c-SWCNTs acting as a scattering site. Considering the mobility of carriers in an atomically perfect CNT, a perfect CNT should be a straight tubular structure. The tubular structure constrains carrier transport paths to one dimension. As a result, the carrier mobility appears extremely high. Meanwhile, the carbon materials treated in this paper are defined as a structure with intrinsic or extrinsic defects. When the various molecules (intercalated and/or adsorbed molecules) were located in the c-SWCNT TFT device as well as on the nanotube, the current paths are disturbed by the factors acting as an intermediate and providing other source in the charge transfer. In this case, the conductivity of the device can be fluctuated by charges on the various molecules that may attract or repel the electrons traveling in the nanotubes. Accordingly, the reason for the decrease of the conductivity can be speculated as follows: the carrier mobility is limited by carrier-carrier scattering between the molecules and c-SWCNTs in the active area between the electrodes, as well as by defects.

However, the current I_{DS} of the FET-1 devices expected to have a lower rate in carrier-carrier scattering has been observed higher than the other. From this fact, one can conclude that the approach using the carrier mobility is not appropriate. The result for the FET-1 devices is thought to be attributed to the contribution from the electrochemical area between the electrodes.

Meanwhile, as already demonstrated in Fig. 3, the increase of the c-SWCNT concentration leads to the increase of the surface coverage of the c-SWCNT thin film on the substrate. Moreover, the surface of c-SWCNT thin film with the increment of its concentration

was covered with a considerable amount of impurity molecules. As shown in Fig. 4b, the current I_{DS} of the FET-2 devices with high density was found to be lower than that of the FET-1 devices.

From the above facts, the second assumable reason for the decrease of the current I_{DS} is that the molecules located on the c-SWCNT surface may change the carrier density and also the effect leads to the decrease of the conductivity in the c-SWCNT TFT devices. For example, if an electron transfers from the adsorbed molecules to a p-type c-SWCNT, the electron will recombine with a hole in the p-type c-SWCNT, and the number of holes will be decreased. From this assumption, it can be derived that the conductivity of the c-SWCNT TFT devices is dropped by the role of the carrier density control due to the interaction between adsorbed molecules and c-SWCNTs.

Figure 5 shows the electrical properties of the FET-3 devices, with structural properties of p-SWCNT and c-SWCNT samples by Raman spectroscopy. The drain characteristics of FET-3 devices for different gate voltages are shown in Fig. 5a. Considering the features of the $I_{DS}-V_{DS}$ curves in this figure, the FET-3 devices were classified as possessing a schottky contact. The reason is that the curves possess the presence of an inflection point near $V_D = 0$ with linear regions on either side for positive and negative drain bias.[49] As shown in the inserted figure of Fig. 5a, the comparison between this result and the results in Figs. 4a and 4c shows that all our devices are dominated by a schottky contact. The comparison also indicates that the c-SWCNT thin film with a high density is more resistive than the other films.

Figure 5b shows a plot of the source-drain current versus gate voltage ($I_{DS}-V_G$) for different source-drain bias conditions. In this figure, the currents I_{DS} as a function of V_{DS} were observed to be saturated near the positive gate voltages. The gate dependence exhibits very weak semiconducting p-type behavior. This characteristic of gate dependence indicates that the field effect response by gate modulation disappears. The similar results were observed in the results of the other groups.[19,50–52]

As shown in figures from Figs. 4 to 5, the electrical characteristics of all our devices have been identified as having a tendency for a disappearance of gate modulation effects with a reduction in the drain currents.

The Raman result in Fig. 5c was introduced to elucidate the reasons for the electrical characteristics observed in our devices. Especially, Fig. 5c shows the normalized spectra to the G-band intensity of Raman spectra plotted in Fig. 2a. The D-band of c-SWCNT in this figure was observed to shift toward higher frequencies with an increase of intensity than that of p-SWCNT. In the analysis of Raman spectra, the increase of the D-band intensity reveals the degradation of the crystalline quality due to the defects. Based on this fact, it can be said that the result on the D-band in Fig. 5c is because of the structural changes by the defects incoming in the process of acid treatment. The structural change is generated by the combination between vacancies in the nanotube lattice and molecules such as COOH groups, CCFs intercalated into the nanotube, i.e., the vacancy-adatom complex.[47]

As a kind of defects, the term 'vacancy-adatom complex' has been used as a concept indicating the functional groups and/or some of extra atoms coupled with the vacancies in the nanotube lattice.[47] In the previous papers, the roles of vacancy-adatom complex are described as follows; (1) a vacancy-adatom complex led to the creation of a pair of deep levels acting as a recombination center of charge carriers inside the energy gap.[47,53] (2) deep levels in the semiconductor band gap retain the ability to induce the decrease of charge carriers.[47] (3) even a low concentration of vacancies in SWCNTs can produce a large decrease in their electrical conductance.[53,54]

From the definition of the role of the vacancy-adatom complex, it can be inferred that the electronic band structure of p- SWCNTs is modified by the deep levels created by the vacancy-adatom complex. This indicates that the vacancy-adatom complex is applied as the same role with dopants.[53] Therefore, it can be concluded that the

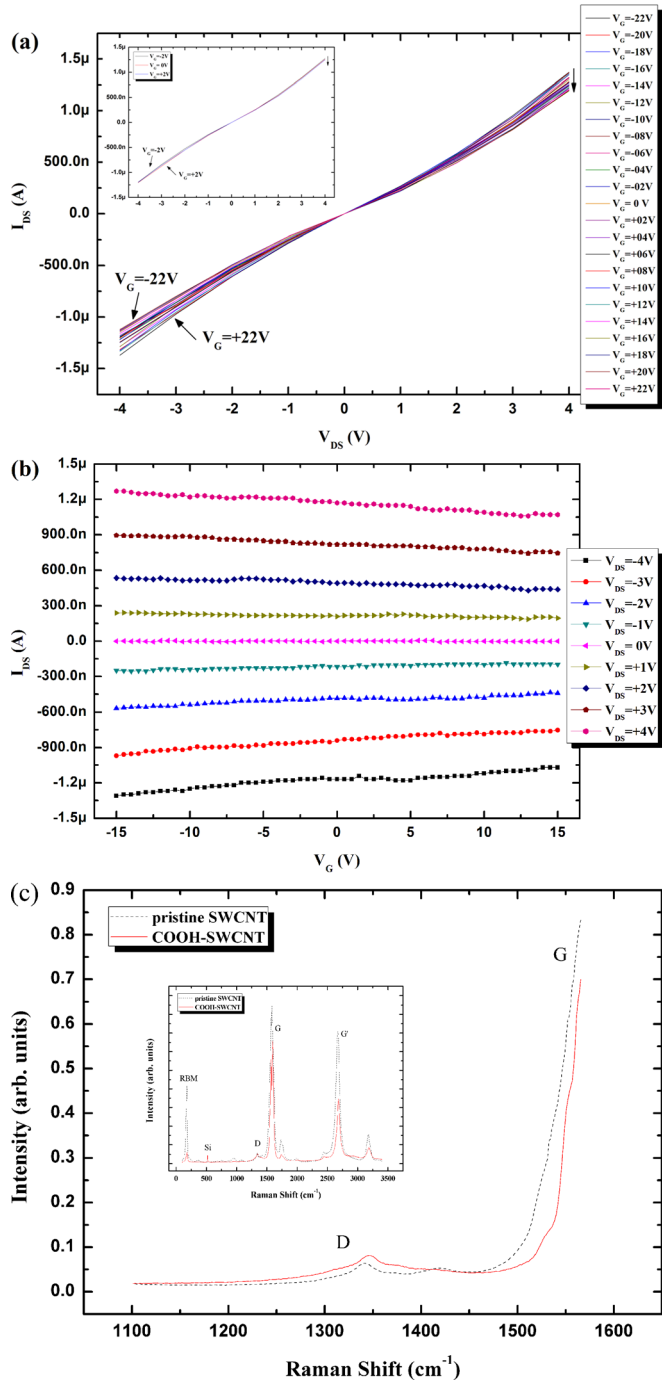

Figure 5. (Color online) The electrical characteristics for c-SWCNT thin film transistor using a suspension with a concentration of 0.192 mg/ml and the normalized Raman spectra from pristine SWCNT and c-SWCNT. (a) current-voltage characteristics between source and drain electrodes, (b) current-gate voltage characteristics (FET-3 device), and (c) the normalized Raman spectra.

RBM shift generated without the dopants in Fig. 2b is attributed to the presence of the deep levels created by the vacancy-adatom complex. Besides, from the second fact that the deep levels lead to the decrease of charge carriers, it can be concluded that a reduction of the drain current arises from the increase of the influence of deep levels by the increment of c-SWCNT concentration.[47] This is consistent with the assumption in Fig. 4 applied for the analysis on the conductivity of the c-SWCNT TFTs.

Meanwhile, the disappearance phenomenon of gate modulation effect was described on the basis of the $I_{DS}-V_G$ properties measured from the FET-1 and FET-2 devices. As shown in Fig. 4, the conversion from ambipolar to a very weak p-type behavior indicates that the holes are a charge carrier of the electronic conduction in the FET-2 devices. Linking this result with the fact that the density of deep levels is increased as the c-SWCNT concentration increases, it can be inferred that the increased deep levels leads to the attenuation of electron flow, which activates the conduction by holes. The activation of the hole conduction indicates that the deep levels act as an acceptor. Therefore, the attenuation of the gate modulation effect is considered because of the deep levels behaving like an acceptor.

In order to study the charge transfer occurring between the defected SWCNTs and the COOH groups, the Raman results in the Figs. 2b and 2c were compared with the electrical characteristics of the devices. The Raman results in the Figs. 2b and 2c show the upshift of RBM and the blueshift of G^+ band, respectively. According to the previous reports, the RBM shift appears when the electronic band structure of SWCNT is modified by the intercalation of acid molecules or dopant atoms into the nanotube bundles.[27–32] The RBM upshift has been reported to be observed when the charge transfer process occurs from carbon-based materials to the acceptor molecules.[27]

As already mentioned in Fig. 2c, the blueshift of G^+ band indicates that the charge transfer between nanotubes and COOH groups consisting of c-SWCNT is dominated by the p-type doping behavior. Until now the predicted results in Fig. 2 coincide with the electrical characteristics of p-type doping behavior obtained from the devices. Thus, it can be concluded that the charge transfer occurred from the defected nanotubes to the –COOH groups.

According to the results described in Figs. 4 and 5 so far, it can be concluded as the following: the conductivity of the c-SWCNT TFTs is suppressed by the recombination of charge carriers generated in both vacancy-adatom complex and the nanotubes.

Additionally, the conductivity of the c-SWCNT TFTs can be influenced by the local impurity and point defects such as photoresist, metal particle, oxygen and etc., as the factors added in the device fabrication process.[55] However, there is a problem that a complete removal of the impurity is difficult.

Meanwhile, the devices examined in this study display lower performance than the conventional devices. To diagnose the cause of this problem, the contact angles in the interface of both APTES coated SiO_2 surface and Au on the APTES were considered. The average water contact angles on APTES coated SiO_2 surface and Au electrodes were observed as 60.5 and 55.2°, respectively. From the fact that the contact angle of Au on the APTES in the literature is about 47°, these differences in wettability are thought to provide the poor electrical contact between c-SWCNT thin films and Au electrodes.[56]

Conclusions

In this work, the electronic properties of c-SWCNT TFT devices have been studied with the structural properties of the chemically treated SWCNTs obtained using Raman spectroscopy. The drain currents and gate modulation effect on the c-SWCNT TFTs have been observed to reduce as the concentration of c-SWCNT is increased. Through the combination of Raman results and transport characteristics of c-SWCNT TFTs, it can suggested that the transport mechanism of these devices is associated with the existence of deep levels produced by vacancy-adatom complex, as an impurity intercalated into the crystalline structure of p-SWCNT.

Acknowledgments

This research has been supported by KIST Basic R&D Projects sponsored by the Korea Institute of Science and Technology (KIST). The authors would like to acknowledge for valuable discussion and helpful comments of Dr. Sang-Myung Lee and Byung Chul Lee.

References

1. N. Saran, K. Parikh, D.-S. Suh, E. Muñoz, H. Kolla, and S. K. Manohar, *J. Am. Chem. Soc.*, **126**, 4462 (2004).
2. Z. Wu, Z. Chen, X. Du, J. M. Logan, J. Sippel, M. Nikolou, K. Kamaras, J. R. Reynolds, D. B. Tanner, A. F. Hebard, et al., *Science*, **305**, 1273 (2004).
3. M. Kaempgen, G. S. Duesberg, and S. Roth, *Appl. Surf. Sci.*, **252**, 425 (2005).
4. A. Schindler, J. Brill, N. Fruehauf, J. P. Novak, and Z. Yaniv, *Phys. E.*, **37**, 119 (2007).
5. K. Bradley, J.-C. P. Gabriel, and G. Grüner, *Nano Lett.*, **3**, 1353 (2003).
6. E. S. Snow, J. P. Novak, M. D. Lay, E. H. Houser, F. K. Perkins, and P. M. Campbell, *J. Vac. Sci. Tech. B*, **22**, 1990 (2004).
7. G. Grüner, *Anal. Bioanal. Chem.*, **384**, 322 (2006).
8. E. Artukovic, M. Kaempgen, D. S. Hecht, S. Roth, and G. Grüner, *Nano Lett.*, **5**, 757 (2005).
9. M. E. Itkis, F. Borondics, A. Yu, and R. C. Haddon, *Science*, **312**, 413 (2006).
10. B. L. Allen, P. D. Kichambare, and A. Star, *Adv. Mater.*, **19**, 1439 (2007).
11. D. Lee and T. Cui, *J. Vac. Sci. Tech. B*, **27**, 842 (2009).
12. M. Kaempgen and S. Roth, *J. Electroanal. Chem.*, **586**, 72 (2006).
13. K. Parikh, K. Cattanach, R. Rao, D.-S. Suh, A. Wu, and S. K. Manohar, *Sens. Actuators B*, **113**, 55 (2006).
14. D. A. Jack, C.-S. Yeh, Z. Liang, S. Li, J. G. Park, and J. C. Fielding, *Nanotechnology*, **21**, 195703 (2010).
15. E. Gracia-Espino, G. Sala, F. Pino, N. Halonen, J. Luomahaara, J. Mäklin, G. Tóth, K. Kordás, H. Jantunen, M. Terrones, et al., *ACS Nano*, **4**, 3318 (2010).
16. M. R. Noor, S. Goyal, S. M. Christensen, and S. M. Iqbal, *Appl. Phys. Lett.*, **95**, 073703 (2009).
17. J. Mäklin, T. Mustonen, N. Halonen, G. Tóth, K. Kordás, J. Vähäkangas, H. Moilanen, Á. Kukovecz, Z. Kónya, H. Haspel, et al., *Phys. Status Solidi B*, **245**, 2335 (2008).
18. T. Mustonen, J. Mäklin, K. Kordás, N. Halonen, G. Tóth, S. Saukko, J. Vähäkangas, H. Jantunen, S. Kar, P. M. Ajayan, et al., *Phys. Rev. B*, **77**, 125430 (2008).
19. Z.-B. Zhang, J. Li, A. L. Cabezas, and S.-L. Zhang, *Chem. Phys. Lett.*, **476**, 258 (2009).
20. C.-M. Yang, J. S. Park, K. H. An, S. C. Lim, K. Seo, B. Kim, K. A. Park, S. Han, C. Y. Park, and Y. H. Lee, *J. Phys. Chem. B*, **109**, 19242 (2005).
21. J.-A. Lee, B. C. Lee, S.-M. Lee, K.-K. Paek, B.-K. Ju, Y.-H. Lee, and H. J. Shin, *J. Electrochem. Soc.*, **157**, K131 (2010).
22. W. Zhao, C. Song, and P. E. Pehrsson, *J. Am. Chem. Soc.*, **124**, 12418 (2002).
23. S. Myung, M. Lee, G. T. Kim, J. S. Ha, and S. Hong, *Adv. Mater.*, **17**, 2361 (2005).
24. M. E. Sandison, S. A. Cumming, W. Kolchbc, and A. R. Pitt, *Lab Chip*, **10**, 2805 (2010).
25. X. Song, J. Zhai, Y. Wang, and L. Jeing, *J. Colloid Interface Sci.*, **298**, 267 (2006).
26. J. Kim, P. Seidler, L. S. Wan, and C. Fill, *J. Colloid Interface Sci.*, **329**, 114 (2009).
27. E. B. Barros, A. G. S. Filho, V. Lemos, J. M. Filho, S. B. Fagan, M. H. Herbst, J. M. Rosolen, C. A. Luengo, and J. G. Huber, *Carbon*, **43**, 2495 (2005).
28. W. Zhou, J. Vavro, N. M. Nemes, J. E. Fischer, F. Borondics, K. Kamarás, and D. B. Tanner, *Phys. Rev. B*, **71**, 205423 (2005).
29. C. Bower, A. Kleinhammes, Y. Wu, and O. Zhou, *Chem. Phys. Lett.*, **288**, 481 (1998).
30. G. U. Sumanasekera, J. L. Allen, S. L. Fang, A. L. Loper, A. M. Rao, and P. C. Eklund, *J. Phys. Chem. B*, **103**, 4292 (1999).
31. S. Costa, B. Scheibe, M. Rummeli, and E. Borowiak-Palen, *Phys. Status Solidi B*, **246**, 2717 (2009).
32. L. Kavan, M. Kalbáč, M. Zukalová, and L. Dunsch, *J. Phys. Chem. B*, **109**, 19613 (2005).
33. B. Gao, Y. Zhang, J. Zhang, J. Kong, and Z. Liu, *J. Phys. Chem. C*, **112**, 8319 (2008).
34. M. Burghard, *Surf. Sci. Rep.*, **58**, 1 (2005).
35. H.-Z. Geng, K. K. Kim, C. Song, N. T. Xuyen, S. M. Kim, K. A. Park, D. S. Lee, K. H. An, Y. S. Lee, Y. Chang, et al., *J. Mater. Chem.*, **18**, 1261 (2008).
36. U. J. Kim, C. A. Furtado, X. Liu, G. Chen, and P. C. Eklund, *J. Am. Chem. Soc.*, **127**, 15437 (2005).
37. M. S. Dresselhaus, G. Dresselhaus, R. Saito, and A. Jorio, *Phys. Rep.*, **409**, 47 (2005).
38. H. Kawamoto, T. Uchida, K. Kojima, and M. Tachibana, *Chem. Phys. Lett.*, **432**, 172 (2006).
39. A. Das, A. K. Sood, A. Govindaraj, A. M. Saitta, M. Lazzeri, F. Mauri, and C. N. R. Rao, *Phys. Rev. Lett.*, **99**, 136803 (2007).
40. J. Kürti, V. Zólyomi, M. Kertesz, and G. Sun, *New J. Phys.*, **5**, 125 (2003).
41. J. Kong, and H. Dai, *J. Phys. Chem. B*, **105**, 2890 (2001).
42. S. Li, Y. Yan, N. Liu, M. B. Chan-Park, and Q. Zhang, *Small*, **3**, 616 (2007).
43. C. G. Salzmann, S. A. Llewellyn, G. Tobias, M. A. Ward, Y. Huh, and M. L. Green, *Adv. Mater.*, **19**, 883 (2007).
44. C. Wang, G. Zhou, J. Wu, B.-L. Gu, and W. Duan, *Appl. Phys. Lett.*, **89**, 173130 (2006).
45. Q. Fu and J. Liu, Langmuir, **21**, 1162 (2005).
46. D. E. Johnston, M. F. Islam, A. G. Yodh, and A. T. Johnson, *Nature Mater.*, **4**. 589 (2005).
47. G. Kim, B. W. Jeong, and J. Ihm, *Appl. Phys. Lett.*, **88**, 193107 (2006).
48. G. Gruner, *Anal. Bioanal. Chem.*, **384**, 322 (2006).

49. D. McClain, N. Thomas, S. Youkey, R. Schaller, J. Jiao, and K. P. O'Brien, *Carbon*, **47**, 1493 (2009).
50. H. E. Unalan, G. Fanchini, A. Kanwal, A. D. Pasquier, and M. Chhowalla, *Nano Lett.*, **6**, 677 (2006).
51. G.-H. Jeong, S. Suzuki, and Y. Kobayashi, *Nanotechnology*, **20**, 285708 (2009).
52. J. S. Hwang, H. T. Kim, H. K. Kim, M. H. Son, S. W. Hwang, and D. Ahn, *Phys. Status Solidi B*, **246**, 744 (2009).
53. S. Lee, G. Kim, H. Kim, B.-Y. Choi, J. Lee, B. W. Jeong, J. Ihm, Y. Kuk, and S.-J. Kahng, *Phys. Rev. Lett.*, **95**, 166402 (2005).
54. C. Gómez-Navarro, P. J. De Pablo, J. Gómez-Herrero, B. Biel, F. J. Garcia-Vidal, A. Rubio, and F. Flores, *Nature Mater.*, **4**, 534 (2005).
55. D. Kang, N. Park, J.-H. Ko, E. Bae, and W. Park, *Nanotechnology*, **16**, 1048 (2005)
56. Y. Kim, I. Choi, S. K. Kang, J. Lee, and J. Yi, *Appl. Phys. Lett.*, **86**, 073113 (2005).